RSC Advances

PAPER

View Article Online
View Journal | View Issue

Check for updates

Cite this: *RSC Adv.*, 2018, **8**, 37307

Cytochrome P450-dependent reactive oxygen species (ROS) production contributes to Mn_3O_4 nanoparticle-caused liver injury†

Zongkai Yue,[a] Xiao Zhang,[a] Qilin Yu,[b] Lu Liu[c] and Xiaomeng Zhou*[a]

Mn_3O_4 nanoparticles (NPs) are one of the most important nanomaterials, and have a wide range of applications (*i.e.*, catalysis, solar-electron transformation and molecular adsorption). However, their biological effect remains to be detailed. In this study, we investigated the *in vivo* toxicity of the synthesized Mn_3O_4 NPs using a long-term exposure model. After exposure to the Mn_3O_4 NPs for 60–120 days, rats preferentially accumulated manganese in the livers. Histopathological observation and apoptosis assays revealed that the Mn_3O_4 NPs caused severe liver injury associated with apoptosis. Transcription profiling analysis, immune histochemistry (IHC) staining and western blotting showed that the NPs significantly up-regulated expression of the cytochrome P450 (CYP1A2). Accordingly, the NP-treated livers exhibited high levels of reactive oxygen species (ROS) and oxidative damage. Moreover, ROS scavenging by *N*-acetylcysteine (NAC) attenuated Mn_3O_4 NP-caused liver injury, but had no impact on the expression of CYP1A2. These results indicated that the toxicity of the Mn_3O_4 NPs was attributed to cytochrome P450-dependent ROS accumulation and consequent oxidative damage. This study uncovers the contribution of cytochrome P450-induced oxidative stress to nanotoxicity.

Received 2nd July 2018
Accepted 1st November 2018

DOI: 10.1039/c8ra05633a

rsc.li/rsc-advances

Open Access Article. Published on 06 November 2018. Downloaded on 12/9/2025 2:58:23 AM.
This article is licensed under a Creative Commons Attribution-NonCommercial 3.0 Unported Licence.

Introduction

Manganese oxides are used in a wide range of applications, such as catalysis, solar-electron transformation, molecular adsorption, and magnetic materials.[1,2] Among them, Mn_3O_4 nanoparticles (NPs) are of significance owing to their excellent physiochemical properties.[3–5] Recently, abundant Mn_3O_4 NP-doped nanomaterials were prepared and exhibited marvelous properties in catalysis, energy storage and magnetic bistability, expanding the importance of Mn_3O_4 NPs in materials science.[6–9] The increasing production of Mn_3O_4 NPs requires improved understanding of their potential effects on human health and the ecological system.

To date, only a few studies have investigated the biological effect of Mn_3O_4 NPs on mammals.[10–13] The Mn_3O_4 NPs could be internalized by the mammalian cells, resulting in reactive oxygen species (ROS) accumulation and generating cytotoxicity.[10] However, there is no evidence that ROS production is the reason driving the cytotoxicity of Mn_3O_4 NPs. An *in vivo* study showed that the Mn_3O_4 NPs might cause dysfunction of the kidneys and the brain, while the mechanism leading to this dysfunction was not explored.[13] Hence, it is highly desirable to investigate the detailed mechanisms of Mn_3O_4 NP-caused toxicity both *in vitro* and *in vivo*.

Cytochromes P450 constitute a group of oxygenases that catalyze oxidative transformation of exogenous and endogenous compounds.[14,15] These enzymes, mainly localized in the endoplasmic reticulum (ER) of the liver cells,[16,17] play a critical role in efficient elimination of foreign chemical agents (*i.e.*, toxins, drugs and heavy metals) from the body.[18] It has been recognized that cytochromes P450 (especially CYP1A2) partially contribute to production of intracellular reactive oxygen species (ROS) and lead to oxidative damage.[18–20] Given the extreme small sizes, nanomaterials might be easily internalized into the cells and frequently exposed to cytochromes P450. However, little is known about the link between cytochromes P450 and nanomaterial-induced ROS production.

The aim of this study is to investigate the *in vivo* effect of Mn_3O_4 NPs with long-term exposure (60–120 d) to the mammals, and to explore possible mechanisms of this biological effect. Herein, we find that the injected Mn_3O_4 NPs are preferentially distributed in the livers, resulting in severe liver injury associated with apoptosis. More strikingly, this study further reveals that the Mn_3O_4 NPs cause up-

[a]*Center for Aircraft Fire and Emergency, Civil Aviation University of China, Tianjin 300300, P. R. China. E-mail: zhouxm@nankai.edu.cn*

[b]*Ministry of Education Key Laboratory of Molecular Microbiology and Technology, College of Life Science, Nankai University, Tianjin 300071, P. R. China*

[c]*Tianjin Key Laboratory of Environmental Remediation and Pollution Control, College of Environmental Science and Engineering, Nankai University, Tianjin 300071, P. R. China*

† Electronic supplementary information (ESI) available. See DOI: 10.1039/c8ra05633a

Open Access Article. Published on 06 November 2018. Downloaded on 12/9/2025 2:58:23 AM.
This article is licensed under a Creative Commons Attribution-NonCommercial 3.0 Unported Licence.

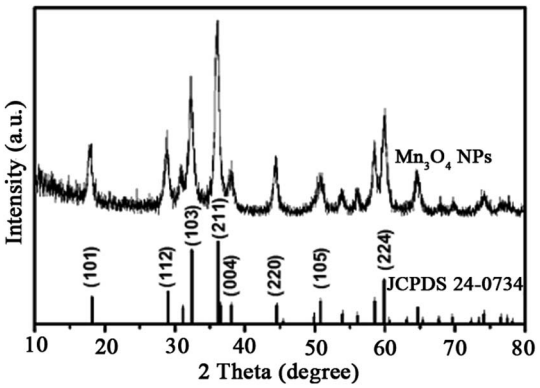

Fig. 1 XRD pattern of the Mn_3O_4 NPs that is consistent with the standard card of Mn_3O_4 (JCPDS 24-0734).

regulation of cytochrome P450, followed by remarkable ROS accumulation and oxidative damage that contributes to the toxicity.

Materials and methods

Synthesis and characterization of Mn_3O_4 NPs

The Mn_3O_4 NPs were synthesized according to Liu's method.[21] The obtained NPs were characterized by transmission electron microscopy (TEM, TecnaiG2 F-20, FEI, USA) and X-ray diffraction (XRD, D/max-2500, Japan).

Animals and treatment

Healthy adult specific-pathogen-free (SPF) Sprague–Dawley (SD) male rats were employed in this study. The rats (8–9 weeks old, 200–250 g per rat) were purchased from the Center for Experimental Animals of North China University of Science and Technology. For housing of animals, plastic cages filled with hardwood bedding were placed within an air-conditioned (23 ± 2 °C, 30–70% relative humidity) animal room with a 12 h light/dark cycle. The rats had free access to food and water. The animal experiments were approved by the Institutional Animal Care and Use Committee of the Center for Experimental Animals of North China University of Science and Technology.

For treatment of Mn_3O_4 NPs, the NPs were suspended in saline at an initial concentration of 1000 mg L^{-1}. 20 mg kg^{-1} of the Mn_3O_4 NPs were intraperitoneally injected into the rats every week for 0 d (control), 60 d or 120 d. At the indicated time, the rats were euthanized, and the organs (including the liver, kidney, brain and heart) were sampled for further assays.

Manganese determination

The organs sampled from the treated rats were homogenized in the distilled water. The obtained homogenates were digested by 30% HNO_3 solution, and the manganese contents in the digestion liquid were determined using inductively coupled plasma (ICP-AES, Thermo Elemental, USA).

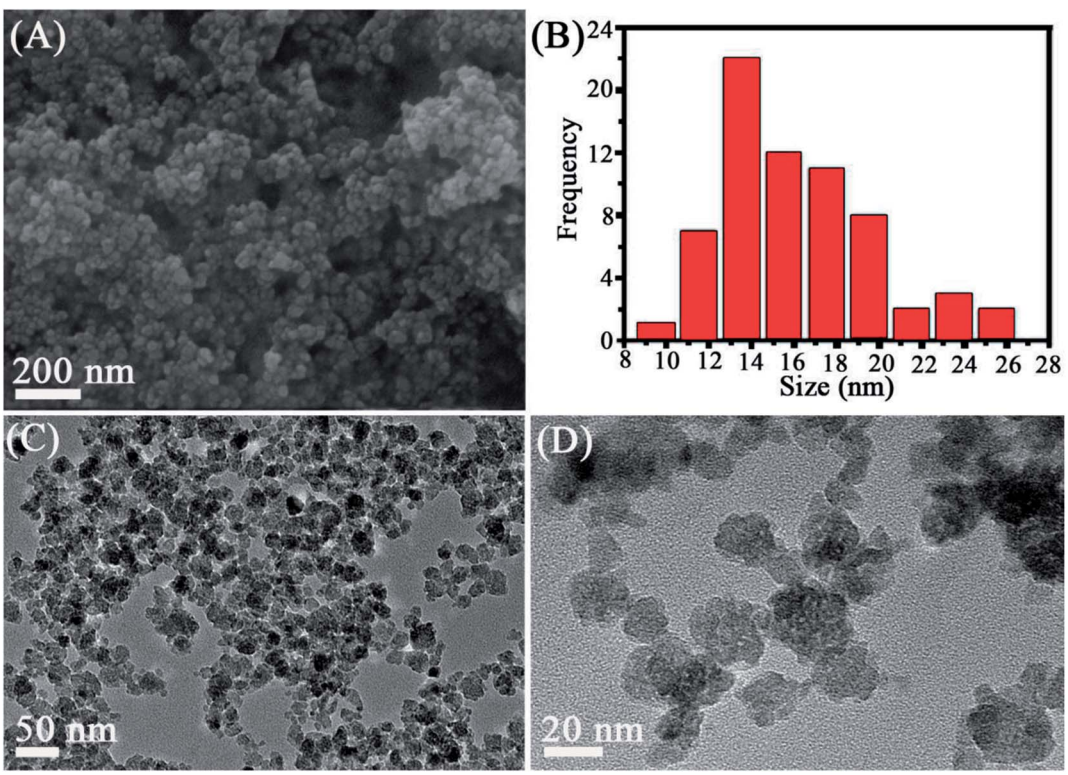

Fig. 2 SEM (A), size distribution (B) and TEM observation (C and D) of the synthesized Mn_3O_4 NPs.

This journal is © The Royal Society of Chemistry 2018

Open Access Article. Published on 06 November 2018. Downloaded on 12/9/2025 2:58:23 AM.
This article is licensed under a Creative Commons Attribution-NonCommercial 3.0 Unported Licence.

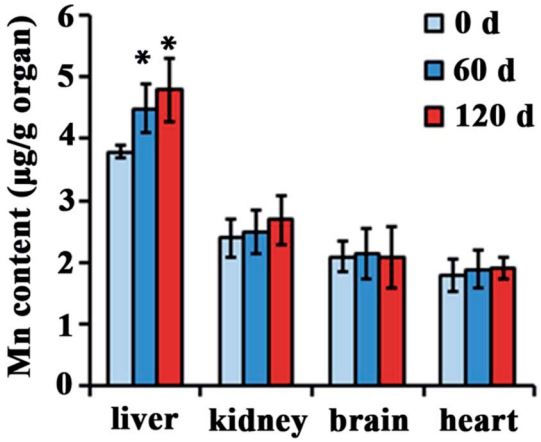

Fig. 3 Manganese contents in various organs of the rats treated by the Mn_3O_4 NPs for indicated time. The values represent the means ± standard deviation ($n = 3$). *Indicates significant difference between the treatment group and the control ($P < 0.05$).

Histopathological analysis and immunohistochemistry (IHC) assay

The selected liver tissues were fixed in 4% paraformaldehyde, embedded in paraffin, cut into 4 μm slices and mounted on glass microscope slides. Thin sections were stained with haematoxylin-eosin (H&E). The slides were then sealed and examined by light microscopy (BX-51, Olympus, Japan). For IHC assay of CYP1A2 and Sult2a1, the sections were stained with the corresponding antibodies (Abcam, USA), and then stained using an IHC kit (Dingguo, China). The stained slides were also examined by the light microscope.

Apoptosis assay

Apoptosis of the liver cells was examined using an FITC-AnnexinV/PI Apoptosis Kit (SungeneBiotech, China).[22] The freshly sampled livers were homogenized in the PBS buffer, and the homogenates were filtered with cell strainers. The isolated cells were stained by FITC-AnnexinV/PI and used for apoptosis assay. The fluorescence intensity of the stained cells was assessed by a flow cytometer (CaLibar, Beckton Dickson, USA), and the percent of apoptotic cells was recorded.

Western blotting

To detect the apoptosis markers (including caspase-3, Bax and Bcl-2)[23] and the ER stress reporting protein GRP78,[24] total proteins were extracted from the liver tissues using RIPA buffer (containing protease inhibitor cocktail), and then separated by SDS-PAGE. The proteins were then transferred into the polyvinylidene fluoride membrane, and the proteins were detected using corresponding antibodies (Abcam, USA).

Transcription profiling analysis

To investigate the transcription profiling in the sampled livers, the total RNAs were extracted from the livers using the Trizol agent. The obtained RNAs were used to generate double-stranded cDNA using the SMARTTMcDNA Library Construction Kit (Clontech, USA). The obtained cDNAs were then used to construct a 454 library. Roche GS-FLX 454 pyrosequencing was conducted by IlluminaHiSeq™2000 (Oebiotech Company in Shanghai, China). Gene annotations were retrieved from the rat genome database (http://rgd.mcw.edu). Assignment of Gene Ontology (GO) and Kyoto Encyclopedia of Genes and Genomes (KEGG) terms was based on JGI annotations. Enrichment of differentially regulated genes in GO and KEGG were determined using GOSeq.

ROS, malonaldehyde (MDA), GSH and total SOD (T-SOD) assays

To examine ROS levels in the liver tissues, the liver cells were obtained by homogenization in the PBS buffer, and stained by 10 μM dihydroethidium (DHE, Invitrogen, USA) for 30 min. The stained cells were washed twice with PBS, and the fluorescence intensity of DHE was determined by a fluorescence microplate reader (PerkinElmer, USA, excitation wavelength 300 nm, emission wavelength 610 nm). Moreover, the oxidative stress-related indicators in the obtained cells, including malonaldehyde (MDA), GSH and T-SOD, were further detected using the MDA assay kit (Jiancheng, China), GSH assay kit (Beyotime, China) and T-SOD assay kit (KeyGEM, China), respectively.

Statistical analysis

Each experiment was performed with three replicates, and the values represent the means ± standard deviations (SD) of three experiments. Difference between the groups were compared by Student's t-test ($P < 0.05$). All statistical tests were performed using the SPSS Statistics Software (V20, IBM, USA).

Results and discussion

Characterization of the synthesized Mn_3O_4 NPs

The structure and morphology of the as-prepared Mn_3O_4 samples were determined by XRD, SEM and TEM. The crystalline-phase structure of as-prepared Mn_3O_4 samples was performed by XRD. XRD patterns revealed that all diffraction peaks of Mn_3O_4 samples are sharp and in a good line with the reported data (JCPDS card, no. 24-0734), indicative of the good crystallization and crystalline-phase of as-prepared samples. No other crystalline-phase was observed in the XRD patterns, confirming that the obtained particles were pure Mn_3O_4 NPs (Fig. 1). SEM (Fig. 2A and S1†) and TEM observation (Fig. 2C and D and S2†) showed that the synthesized Mn_3O_4 samples presented the morphology of uniform and monodispersed nanoparticles, and no obvious accumulation was observed. Fig. 2C and D illustrate high magnification TEM surface morphology and particle size distribution of Mn_3O_4 NPs. It was observed that Mn_3O_4 NPs had particle sizes of 10–25 nm, with the mean size of 15 nm. In the following experiments, we used the synthesized Mn_3O_4 NPs for investigation of biological effects.

Mn_3O_4 NPs lead to specific manganese accumulation in the rat liver

Distribution of NPs in the body is closely associated with their biological effect. To investigate distribution after injected with

Open Access Article. Published on 06 November 2018. Downloaded on 12/9/2025 2:58:23 AM.
This article is licensed under a Creative Commons Attribution-NonCommercial 3.0 Unported Licence.

Mn_3O_4 NPs, different organs of rats, such as the liver, kidney, brain, lung, heart and testicle, were isolated and used for manganese determination. There is no significant difference in manganese content of kidney, brain, lung, heart and testicle between the control and the Mn_3O_4 NP-treated rats. Interestingly, the livers of the Mn_3O_4 NP-treated rats had significant higher manganese contents than that of the control, and prolonged treatment time (120 d) led to increased manganese contents of the livers (Fig. 3). Therefore, the Mn_3O_4 NPs had preferential accumulation in the rat livers.

Mn_3O_4 NPs cause severe liver injury

Since the Mn_3O_4 NPs were preferentially accumulated in the livers, we suggested that the NPs might most likely have an impact on this organ. To verify this, histopathological observation of the NP-treated livers was performed. For the liver tissues of the rats at the 0 day (control), the tissues had normal hepatocytes and sinus hepaticus. The hepatocytes were arranged radically from the central vein, exhibiting clear frames and regular cell structures (Fig. 4A, 0 d). In contrast, the liver tissues after 60 days of treatment showed obvious inflammatory cell infiltration, with widened intercellular spaces and irregular veins (Fig. 4A, 60 d). More strikingly, the tissues after 120 days of treatment had severe inflammation, with remarkably damaged veins and exfoliated cells (Fig. 4A, 120 d).

To further confirm liver injury caused by the Mn_3O_4 NPs, apoptosis of liver cells was examined. Flow cytometry demonstrated that the liver cells isolated from the treated rats exhibited obvious apoptosis as compared to the control (13–

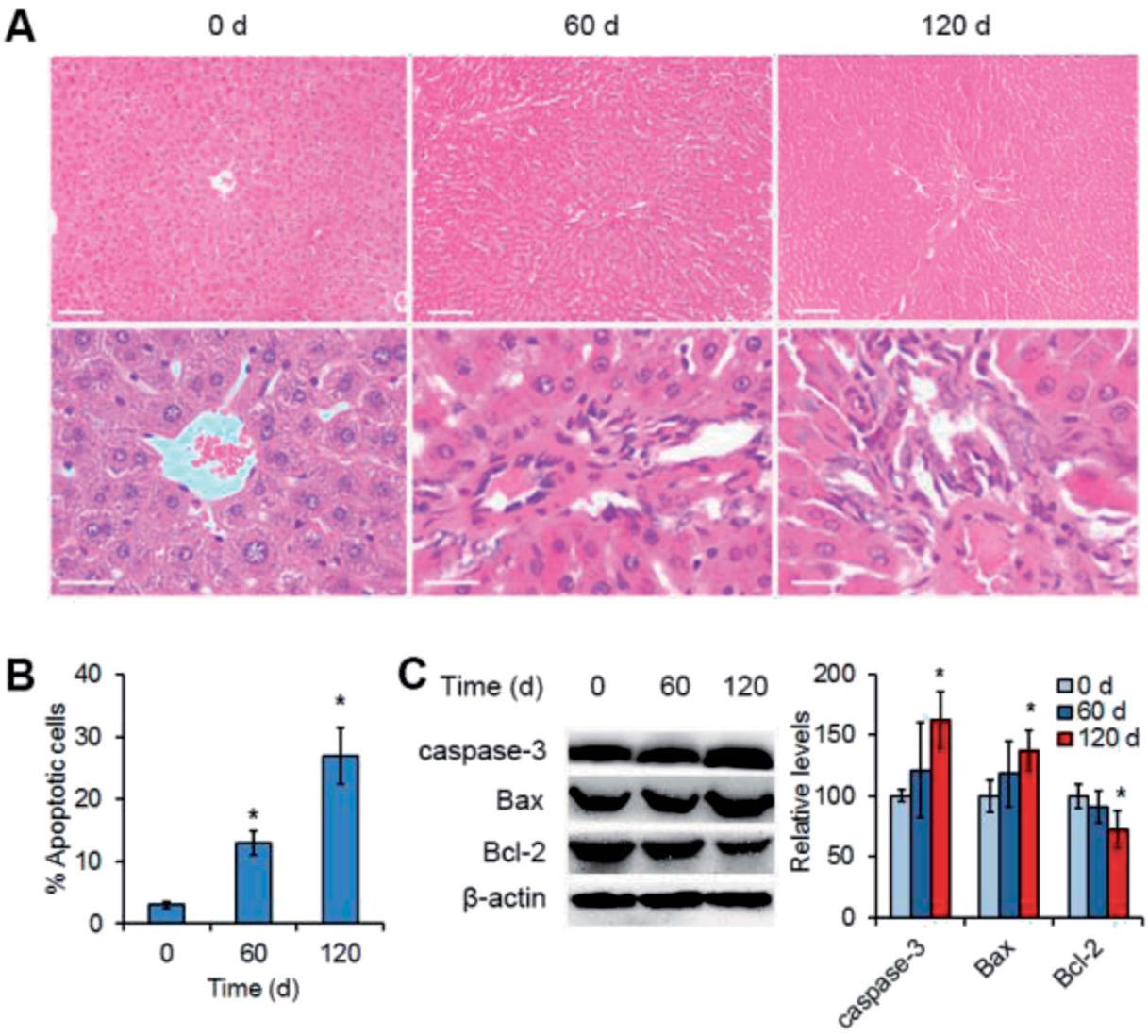

Fig. 4 Mn_3O_4 NPs cause liver injury as revealed by both histopathological observation (A) and apoptosis analysis (B and C). (A) Histopathological images of the liver tissues after treatment of Mn_3O_4 NPs. The treated livers were fixed, sectioned, stained by the hematoxylin and eosin (H&E) reagents, and observed by light microscopy. Scale bars = 100 μm (up) or 50 μm (down). (B) Flow cytometry of liver cells isolated from the treated livers. The cells were stained by AnnexinV and propidium iodide (PI), and then were examined by flow cytometry. (C) Western blotting of the apoptosis markers, including caspase-3, Bax and Bcl2. The values represent the means ± standard deviation (n = 3). *Indicates significant difference between the treatment group and the control ($P < 0.05$).

 This journal is © The Royal Society of Chemistry 2018

Open Access Article. Published on 06 November 2018. Downloaded on 12/9/2025 2:58:23 AM.
This article is licensed under a Creative Commons Attribution-NonCommercial 3.0 Unported Licence.

27% *versus* 3%) (Fig. 4B). Western blotting further revealed the significant increased levels of the apoptosis-inducing factors caspase-3 and Bax, and the decreased levels of the apoptosis-inhibiting factor Bcl-2 in the livers after 120 day treatment of the Mn_3O_4 NPs (Fig. 4C). Taken together, Mn_3O_4 NPs had a strong impact on the liver tissues and led to severe liver injury associated with apoptosis.

Mn_3O_4 NPs up-regulate expression of cytochrome P450 and GRP78 in the liver

To investigate the toxicity mechanism of Mn_3O_4 NPs to the rat livers, transcription profiling analysis of both the untreated and treated livers was performed. Treatment of the NPs only led to up-regulation of a few genes, and this up-regulation was enhanced after 120 days of treatment. Especially, KEGG analysis

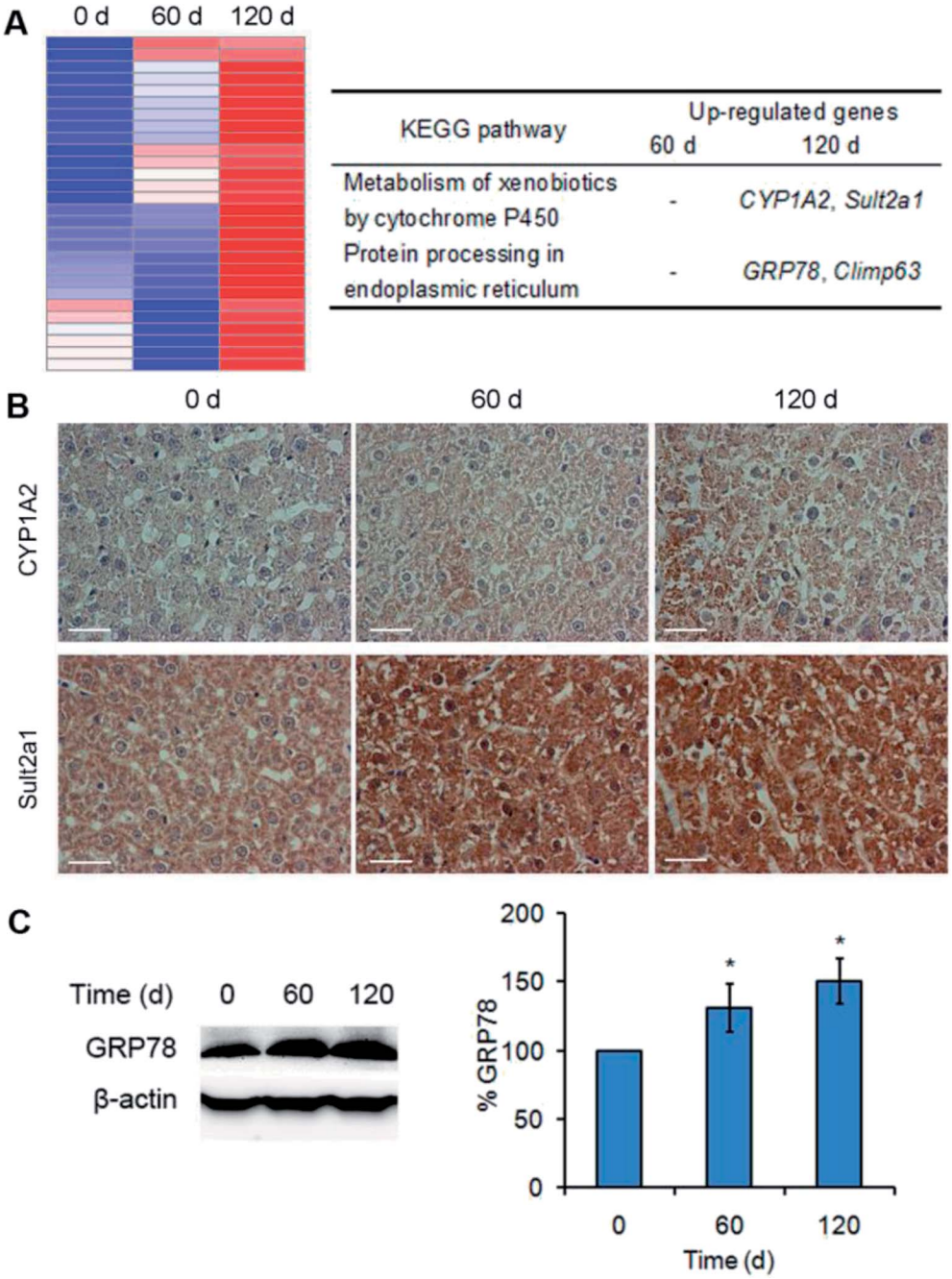

Fig. 5 Mn_3O_4 NPs up-regulate cytochrome P450 and activate the UPR pathway. (A) Transcription profiling analysis of the livers treated by Mn_3O_4 NPs. The left image is the hot map indicative of up-regulation of several genes. The right table indicates two KEGG pathways and corresponding up-regulated genes. (B) IHC images of CYP1A2 and Sult2a1. (C) Western blotting images and statistical analysis of GRP78. The values represent the means ± standard deviation ($n = 3$). *Indicates significant difference between the treatment groups and the control ($P < 0.05$).

Open Access Article. Published on 06 November 2018. Downloaded on 12/9/2025 2:58:23 AM.
This article is licensed under a Creative Commons Attribution-NonCommercial 3.0 Unported Licence.

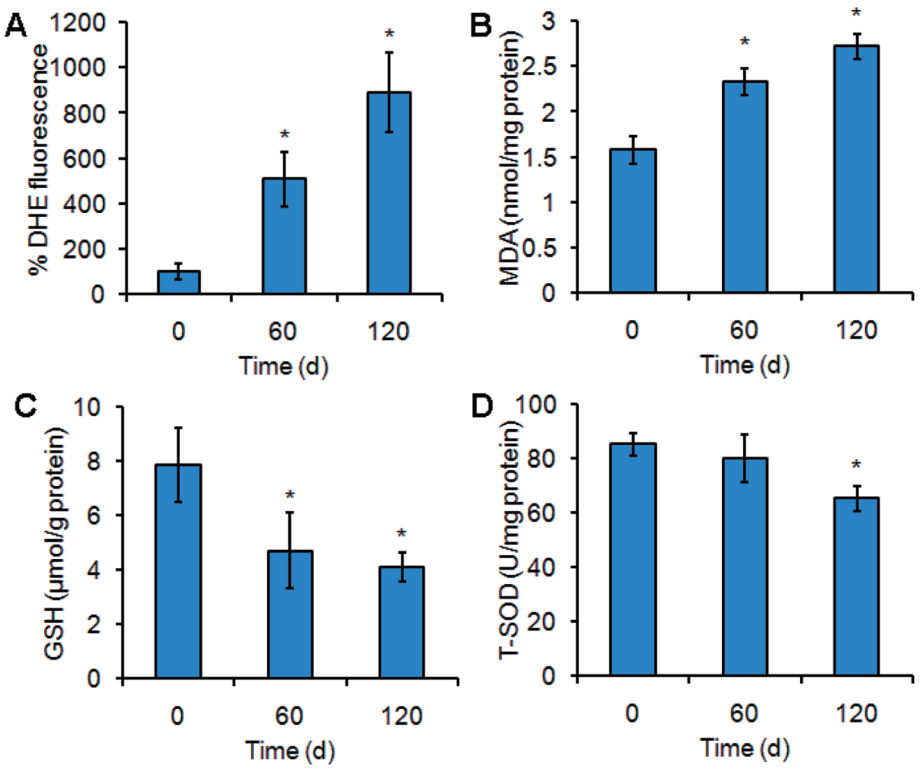

Fig. 6 Mn_3O_4 NPs lead to ROS production and have an impact on oxidative stress-related indicators. (A) ROS levels in the livers of the rats treated by Mn_3O_4 NPs or not. The ROS levels are indicated by DHE fluorescence intensity. (B) MDA contents of the treated livers. (C) GSH contents of the treated livers. (D) T-SOD activity of the treated cells. The values represent the means ± standard deviation ($n = 3$). *Indicates significant difference between the treatment group and the control ($P < 0.05$).

revealed that two pathways were activated by the NPs after 120 days of treatment, including metabolism of xenobiotics by cytochrome P450 (indicated by up-regulation of *CYP1A2* and *Sult2a1*) and protein processing in endoplasmic reticulum (indicated by up-regulation of *GRP78*, *Climp63*) (Fig. 5A). IHC assay and western blotting further confirmed that the corresponding proteins, such as CYP1A2 (cytochrome P450), Sult2a1 and GRP78, had increased levels in the treated liver tissues (Fig. 5B and C). These results suggested that Mn_3O_4 NPs not only increased cytochrome P450 levels, but also led to the activation of unfolded protein response (UPR, indicated by up-regulation of *GRP78* and *Climp63*), an indicator of ER stress. Given that the cytochrome P450 is mainly localized in the ER, it was most likely that the increased activity of cytochrome P450 might further result in ER stress, followed by activation of the UPR pathway.

Mn_3O_4 NPs lead to remarkable oxidative stress in the liver

Cytochrome P450 is frequently associated with ROS production.[18–20] As shown in Fig. 4, Mn_3O_4 NPs up-regulated the levels of cytochrome P450. We hypothesized that this up-regulation caused by the NPs might be accompanied with ROS accumulation. To verify this, the ROS levels in liver cells were detected by DHE staining. As expected, treatment of Mn_3O_4 NPs led to significant increase of intracellular ROS levels, as indicated by the drastic DHE fluorescence intensity in the treated livers (Fig. 6A).

ROS production may cause oxidative damage of the plasma membrane, leading to generation of MDA.[25] MDA assays of the liver tissues further revealed that the MDA contents in the NP-treated livers were higher than the MDA contents in the control (Fig. 6B). Moreover, the treated livers exhibited lower contents of the antioxidant factor GSH and decreased activity of total SOD (T-SOD) (Fig. 6C and D), implying that Mn_3O_4 NPs had an impact on the antioxidant systems. These results indicated that the Mn_3O_4 NPs caused severe oxidative stress, resulting in oxidative damage and impairment of the antioxidant systems in the liver tissues.

ROS scavenging attenuates Mn_3O_4 NP-induced liver injury

To explore the contribution of ROS in Mn_3O_4 NP-induced liver injury, an ROS scavenger, *N*-acetylcysteine (NAC) was intravenously injected into the Mn_3O_4 NP-treated rats, and the livers were then sampled for further assays. Expectedly, NAC could remarkably reduce the NP-caused ROS production in the livers (Fig. 7A), followed by attenuation of NP-induced apoptosis (Fig. 7B). Therefore, ROS accumulation played the critical role in Mn_3O_4 NP-induced liver injury.

The effect of ROS scavenging on expression of CYP1A2 (cytochrome P450), CYP1A2 activity assays, and GRP78 was further examined. Interestingly, NAC injection had no impact

 This journal is © The Royal Society of Chemistry 2018

Open Access Article. Published on 06 November 2018. Downloaded on 12/9/2025 2:58:23 AM.
This article is licensed under a Creative Commons Attribution-NonCommercial 3.0 Unported Licence.

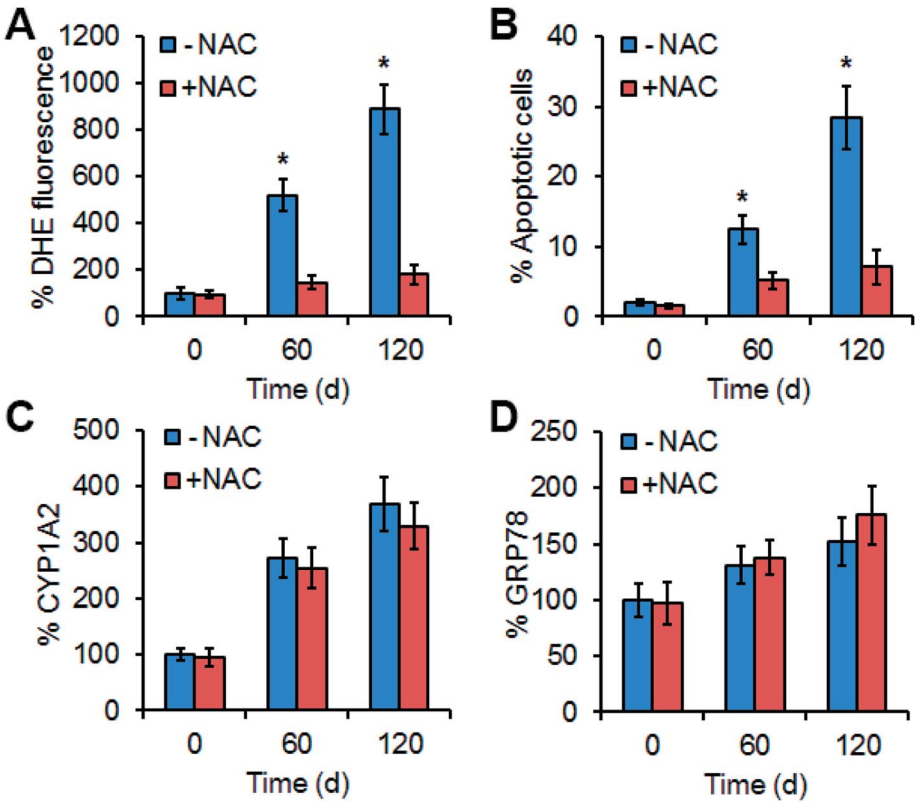

Fig. 7 Effect of the ROS scavenger NAC on ROS accumulation (A), apoptosis (B) and expression of CYP1A2 (C) and GRP78 (D). (A) ROS levels indicated by DHE fluorescence intensity in the livers treated by Mn_3O_4 NP alone (−NAC) or in combination with NAC (+NAC). (B) Apoptosis in the treated livers. (C) Contents of CYP1A2 in the livers, which is examined by Western blotting. (D) Contents of GRP78 in the livers. The values represent the means ± standard deviation ($n = 3$). * indicates significant difference between the treatment group and the control ($P < 0.05$).

on the levels of CYP1A2, CYP1A2 activity assays, and GRP78 in the livers under the treatment of Mn_3O_4 NP (Fig. 7C, D and S3†). This implied that up-regulation of cytochrome P450 in the livers by the Mn_3O_4 NPs led to ROS accumulation, while ROS accumulation did not influence the expression of cytochrome P450.

Conclusion

In conclusion, this study reveals that the Mn_3O_4 NPs preferentially accumulate in the livers, and their long-term exposure causes severe liver injury associated with apoptosis. Further investigations show that the Mn_3O_4 NPs induce up-regulation of cytochrome P450 and ER stress, followed by ROS accumulation and consequent oxidative damage. The oxidative damage is attributable to the Mn_3O_4 NP-induced liver injury. This study uncovers a new mechanism of Mn_3O_4 NP-induced organ injury, and sheds a novel light on the contribution of cytochrome P450-related oxidative stress to nanotoxicity.

Conflicts of interest

There are no conflicts to declare.

Acknowledgements

This work was supported by National Science Foundation of China (No. 51776219), Natural Science Foundation of Tianjin (15JCQNJC15300) and Fundamental Research Funds for the Central Universities (3122018C040).

References

1 W. S. Seo, H. H. Jo, K. Lee, B. Kim, S. J. Oh and J. T. Park, Size-dependent magnetic properties of colloidal Mn_3O_4 and MnO nanoparticles, *Angew. Chem., Int. Ed.*, 2004, **43**, 1115–1117.
2 P. Li, C. Y. Nan, Z. Wei, J. Lu, Q. Peng and Y. D. Li, Mn_3O_4 nanocrystals: facile synthesis, controlled assembly, and application, *Chem. Mater.*, 2010, **22**, 4232–4236.
3 N. N. Zhao, W. Nie, X. B. Liu, S. Z. Tian, Y. Zhang and X. L. Ji, Shape- and size-controlled synthesis and dependent magnetic properties of nearly monodisperse Mn_3O_4 nanocrystals, *Small*, 2008, **4**, 77–81.
4 J. Gao, M. A. Lowe and H. D. Abruna, Spongelike nanosized Mn_3O_4 as a high-capacity anode material for rechargeable lithium batteries, *Chem. Mater.*, 2011, **23**, 3223–3227.
5 E. Winkler, R. D. Zysler and D. Fiorani, Surface and magnetic interaction effects in Mn_3O_4 nanoparticles, *Phys. Rev. B: Condens. Matter Mater. Phys.*, 2004, **70**, 174406.

Open Access Article. Published on 06 November 2018. Downloaded on 12/9/2025 2:58:23 AM. This article is licensed under a Creative Commons Attribution-NonCommercial 3.0 Unported Licence.

6 J. J. Duan, S. Chen, S. Dai and S. Z. Qiao, Shape Control of Mn_3O_4 nanoparticles on nitrogen-doped Graphene for enhanced oxygen reduction activity, *Adv. Funct. Mater.*, 2014, **24**, 2072–2078.

7 H. Liu, Z. H. Li, Y. R. Liang, R. W. Fu and D. C. Wu, Facile synthesis of MnO multi-core@nitrogen-doped carbon shell nanoparticles for high performance lithium-ion battery anodes, *Carbon*, 2015, **84**, 419–425.

8 C. F. Liu, H. Q. Song, C. K. Zhang, Y. G. Liu, C. P. Zhang, X. H. Nan and G. Z. Cao, Coherent Mn_3O_4-carbon nanocomposites with enhanced energy-storage capacitance, *Nano Res.*, 2015, **8**, 3372–3383.

9 M. D. Gimenez-Lopez, A. La Torre, M. W. Fay, P. D. Brown and A. N. Khlobystov, Assembly and magnetic bistability of Mn_3O_4 nanoparticles encapsulated in hollow carbon nanofibers, *Angew. Chem., Int. Ed.*, 2013, **52**, 2051–2054.

10 R. Frick, B. Muller-Edenborn, A. Schlicker, B. Rothen-Rutishauser, D. O. Raemy, D. Gunther, B. Hattendorf, W. Stark and B. Beck-Schimmer, Comparison of manganese oxide nanoparticles and manganese sulfate with regard to oxidative stress, uptake and apoptosis in alveolar epithelial cells, *Toxicol. Lett.*, 2011, **205**, 163–172.

11 A. Ivask, T. Titma, M. Visnapuu, H. Vija, A. Kakinen, M. Sihtmae, S. Pokhrel, L. Madler, M. Heinlaan, V. Kisand, R. Shimmo and A. Kahru, Toxicity of 11 metal oxide nanoparticles to three mammalian cell types *in vitro*, *Curr. Top. Med. Chem.*, 2015, **15**, 1914–1929.

12 T. Titma, R. Shimmo, J. Siigur and A. Kahru, Toxicity of antimony, copper, cobalt, manganese, titanium and zinc oxide nanoparticles for the alveolar and intestinal epithelial barrier cells *in vitro*, *Cytotechnology*, 2016, **68**, 2363–2377.

13 B. A. Katsnelson, I. A. Minigaliyeva, V. G. Panov, L. I. Privalova, A. N. Varaksin, V. B. Gurvich, M. P. Sutunkova, V. Y. Shur, E. V. Shishkina, I. E. Valamina and O. H. Makeyev, Some patterns of metallic nanoparticles' combined subchronic toxicity as exemplified by a combination of nickel and manganese oxide nanoparticles, *Food Chem. Toxicol.*, 2015, **86**, 351–364.

14 R. C. Zangar, D. R. Davydov and S. Verma, Mechanisms that regulate production of reactive oxygen species by cytochrome P450, *Toxicol. Appl. Pharmacol.*, 2004, **199**, 316–331.

15 U. M. Zanger and M. Schwab, Cytochrome P450 enzymes in drug metabolism: Regulation of gene expression, enzyme activities, and impact of genetic variation, *Pharmacol. Ther.*, 2013, **138**, 103–141.

16 F. J. Gonzalez, Role of cytochromes P450 in chemical toxicity and oxidative stress: studies with CYP2E1, *Mutat. Res., Fundam. Mol. Mech. Mutagen.*, 2005, **569**, 101–110.

17 R. J. Edwards, B. P. Murray, A. M. Singleton and A. R. Boobis, Orientation of cytochromes P450 in the endoplasmic reticulum, *Biochemistry*, 1991, **30**, 71.

18 P. Acharya, M. X. Liao, J. C. Engel and M. A. Correia, Liver cytochrome P450 3A endoplasmic reticulum-associated degradation a major role for the p97 AAA ATPase in cytochrome P450 3A extraction into the cytosol, *J. Biol. Chem.*, 2011, **286**, 3815–3828.

19 D. V. Parke, The Cytochromes P450 and Mechanisms of Chemical Carcinogenesis, *Environ. Health Perspect.*, 1994, **102**, 852.

20 P. C. Nair, R. A. McKinnon and J. O. Miners, Cytochrome P450 structure-function: insights from molecular dynamics simulations, *Drug Metab. Rev.*, 2016, **48**, 434–452.

21 F. Jiao and H. Frei, Nanostructured manganese oxide clusters supported on mesoporous silica as efficient oxygen-evolving catalysts, *Chem. Commun.*, 2010, **46**, 2920–2922.

22 I. Vermes, C. Haanen, H. Steffens-Nakken and C. Reutellingsperger, A novel assay for apoptosis flow cytometric detection of phosphatidylserine expression on early apoptotic cells using fluorescein labelled Annexin V, *J. Immunol. Methods*, 1995, **184**, 39–51.

23 E. H. Y. A. Cheng, M. C. Wei, S. Weiler, R. A. Flavell, T. W. Mak, T. Lindsten and S. J. Korsmeyer, BCL-2, BCL-X-L sequester BH3 domain-only molecules preventing BAX- and BAK-mediated mitochondrial apoptosis, *Mol. Cell*, 2001, **8**, 705–711.

24 J. S. Shen, X. Chen, L. Hendershot and R. Prywes, ER stress regulation of ATF6 localization by dissociation of BiP/GRP78 binding and unmasking of golgi localization signals, *Dev. Cell*, 2002, **3**, 99–111.

25 L. Yang, G. Y. Tan, Y. Q. Fu, J. H. Feng and M. H. Zhang, Effects of acute heat stress and subsequent stress removal on function of hepatic mitochondrial respiration, ROS production and lipid peroxidation in broiler chickens, *Comp. Biochem. Physiol. C*, 2010, **151**, 204–208.

 This journal is © The Royal Society of Chemistry 2018